ACCEPTED MANUSCRIPT

Hard X-ray photoelectron and X-ray absorption spectroscopy characterization of oxidized surfaces of iron sulfides

Yuri Mikhlin,[a]* Yevgeny Tomashevich,[a] Sergey Vorobyev,[a,b] Svetlana Saikova,[b] Alexander Romanchenko,[a] Roberto Félix[c]

[a] Institute of Chemistry and Chemical Technology of the Siberian Branch of the Russian Academy of sciences, Akademgorodok, 50/24, Krasnoyarsk, 660036, Russia

[b] Siberian Federal University, Svobodny pr. 79, Krasnoyarsk, 660041, Russia

[c] Renewable Energy, Helmholtz-Zentrum Berlin für Materialien und Energie GmbH, Lise-Meitner-Campus, Hahn-Meitner-Platz 1, 14109 Berlin, Germany

* corresponding author, e-mail: yumikh@icct.ru

ACCEPTED MANUSCRIPT

Highlights

- Pyrite and pyrrhotite in-air abraded and etched in aqueous Fe^{3+} solution were studied
- HAXPES (2 keV-6 keV) and Fe K-, S K-edge XANES (TEY and PFY mode) were measured
- Outer "polysulfide", strongly S-excessive layers are no more than 1-5 nm thick
- "Metal-depleted" layers depend on the treatment and differ for pyrite and pyrrhotite
- Extended nearly-stoichiometric "defective" underlayers were detected using TEY XANES

ACCEPTED MANUSCRIPT

Abstract

Hard X-ray photoelectron spectroscopy (HAXPES) using an excitation energy range of 2 keV to 6 keV in combination with Fe K- and S K-edge XANES, measured simultaneously in total electron (TEY) and partial fluorescence yield (PFY) modes, have been applied to study near-surface regions of natural polycrystalline pyrite FeS_2 and pyrrhotite $Fe_{1-x}S$ before and after etching treatments in an acidic ferric chloride solution. It was found that the following near-surface regions are formed owing to the preferential release of iron from oxidized metal sulfide lattices: (i) a thin, no more than 1-4 nm in depth, outer layer containing polysulfide species, (ii) a layer exhibiting less pronounced stoichiometry deviations and low, if any, concentrations of polysulfide, the composition and dimensions of which vary for pyrite and pyrrhotite and depend on the chemical treatment, and (iii) an extended almost stoichiometric underlayer yielding modified TEY XANES spectra, probably, due to a higher content of defects. We suggest that the extended layered structure should heavily affect the near-surface electronic properties, and processes involving the surface and interfacial charge transfer.

Keywords: HAXPES; XANES; pyrite; pyrrhotite; oxidation; undersurface

ACCEPTED MANUSCRIPT

1. Introduction

Pyrite and pyrrhotite are the most common sulfide minerals of iron. These minerals are frequently found together with non-ferrous base metals and precious metals in ores and play an important role in the biogeochemical sulfur cycle and other environmental processes [1-4]. Pyrite (FeS_2) has a cubic crystal lattice composed of low-spin ferrous iron and disulfide S_2^{2-}groups with a bulk band gap of about 0.95 eV [5-7]; it is one of the promising materials for photovoltaic [8, 9], battery cathode [10, 11], thermoelectric [12] and other applications. Pyrrhotites ($Fe_{1-x}S$, $0 < x < 0.2$) crystallize in a NiAs-like structure consisting of high-spin Fe^{2+}, monosulfide anions and a system of ordered cationic vacancies, having a very narrow gap of about 0.05 eV [1,13,14]. The chemical reactivity of iron sulfides in the environment and during mineral processing, as well as their electronic and optical properties strongly depend on the composition and structure of the real surfaces formed in natural and technological environments. It is known from X-ray photoelectron spectroscopy (XPS) and other surface-sensitive techniques [2-4, 15-34] that iron can be easily released from the lattice of these compounds, leaving non-equilibrium metal-deficient surface layers. The resulting surface sulfur enrichment is generally modest for oxidation-resistant pyrite, with intrinsic (fractured) pyrite surfaces possibly even being S-deficient [2-6, 17-26]. In contrast, the metal depleted layer incorporates di- and polysulfide species and low-spin Fe(II) and can be as thick as several micrometers at pyrrhotite reacted in acidic solutions under certain conditions [27-35]; for example, Pratt and co-workers [30-32] have reported Auger depth profiles of several reacted pyrrhotites. It remains, however, unclear how the undersurface species alter with depth, in particular, because Ar^+ ion sputtering employed in many works could seriously affect the chemical state of Fe and S.

The characterization effectiveness of conventional XPS, which has been widely used to study intrinsic and reacted (oxidized) surfaces of pyrite and pyrrhotite, is limited to photoelectron kinetic energies lower than 1.5 keV, corresponding to inelastic mean free path (IMFP) and information depths (ID = 3 × IMFP) in the order of a few nanometers [37]. Hard X-ray photoelectron spectroscopy (HAXPES) operates in the energy range of photons and emitted electrons of up to 10-15 keV with the IMFP approaching several tens of nanometers [36-40]. HAXPES is a non-destructive technique that allows to determine chemical shifts of core levels and chemical states of the atoms of interest at varying depths. As far as we know, this technique has not yet been applied to reacted iron sulfides, although several studies on related materials, in particular, copper-depleted and copper-rich $Cu(In,Ga)Se_2$ samples [41,42] have been reported.

In the present work, HAXPES was used in combination with X-ray absorption near-edge structure spectroscopy (XANES) measured both in partial fluorescence yield (PFY) and near-

ACCEPTED MANUSCRIPT

surface-sensitive total electron yield (TEY) modes, to probe the unoccupied density of states and the chemical states of the probed elements. A number of XANES studies on iron sulfides have been reported previously [33, 43-56], but the difference between TEY and PFY K-edge spectra of air-oxidized and chemically etched materials has not been analyzed yet. Here, samples of each mineral (i.e., pyrite and pyrrhotite) polished in air were compared with those treated with acidic ferric chloride solution to probe the effect of exposure to the leaching (etching) medium in hydrometallurgy and natural environments, and in materials science. The study revealed "layered" structures of the reacted undersurface both at pyrrhotite and pyrite, even if only oxidized in ambient air, which are expected to exhibit altered electronic and chemical properties.

2. Experimental

Natural pyrite crystals (Ozernoye ore deposit, Russia) without visible inclusions of foreign phases had an average composition of $FeS_{2.0}$ and contained the following impurities (in wt. %, as determined by X-ray fluorescence analysis): Cu 0.14, Si 1.03, Zn 0.11, Ca 0.19. Natural polycrystalline hexagonal pyrrhotite Fe_9S_{10} from a Norilsk ore deposit contained about 2 wt.% impurity of pentlandite, $(Fe,Ni)_9S_8$, as described in detail elsewhere [33-36]. Plates of approximately 2×5×6 mm were cut from the massive minerals, abraded on silicon carbide paper, and then cleaned by wet filter paper to remove fine particles. For oxidative etching, the plates were conditioned in 0.5 M $FeCl_3$ + 0.5 M HCl solutions at 50 $^{\circ}$C for 30 min, rinsed with distilled water and introduced in vacuum.

HAXPES and XANES measurements were carried out at the High Kinetic Energy Photoelectron Spectrometer (HIKE) endstation located at the BESSY KMC-1 beamline at Helmholtz-Zentrum Berlin (HZB). The endstation was operated with a background pressure in the order of 10^{-9} mBar. A Si(1 1 1) double-crystal pair was to monochromatize the energy of the (horizontally-polarized) X-ray beam. The beam intensity was constant, as monitored by a N_2 ionization chamber, in the top-up mode of the storage ring. The monochromator resolution and the flux at the sample varied with photon energy; further details about the experimental setup can be found in refs. [39,40]. Photoemission spectra were collected using a Scienta R4000 hemispherical analyzer modified for high transmission and high resolution at electron kinetic energies up to 10 keV. The analyzer is positioned at about 90^{o} to the incident beam, and the HAXPES spectra were collected using grazing incidence of the photon beam and normal emission of electrons from the sample surface. The survey and the detail HAXPES spectra were recorded at pass energies of 500 eV and 200 eV, respectively. The spectra were acquired at photon energies from 2 keV to 6 keV and, in some cases, to 9 keV; the slit width was of 0.5 mm for

ACCEPTED MANUSCRIPT

all the excitation photon energies. Atomic ratios of elements ($I_{i,h\nu}$) relative to S were calculated from the intensity area of the detail spectra for each energy ($A_{i,h\nu}$) employing photoionization cross-sections ($\sigma_{i,h\nu}$) tabulated in [57,58] and the ones extrapolated for the higher energies, and taking into account IMFP ($\lambda(KE)_i$) calculated for FeS_2 and Fe_9S_{10} employing TPP−2M formula [38] and analyzer's transmission function ($T(KE)_i$) [40-42] using following equation

$$I_{i,h\nu} = A_{i,h\nu} \cdot \sigma_{S,h\nu} \cdot \lambda(KE)_S \cdot T(KE)_S / [A_{S2p,h\nu} \cdot \sigma_{i,h\nu} \cdot \lambda(KE)_i \cdot T(KE)_i].$$

To calibrate the energy scale, the Au $4f_{7/2}$ line of a clean gold foil was measured and set to 84.0 eV. When necessary, the binding energies were corrected for electrostatic charging using the C 1s peak (285.0 eV) from aliphatic carbon contamination. The spectra were fitted after subtraction of a Shirley background with Gaussian-Lorenzian peak shapes using CasaXPS program package (version 2.3.16 PR 1.6). The atomic ratio and S 2p fitting uncertainties were estimated to be within 5-10 %.

X-ray absorption spectra were acquired simultaneously in total electron yield (TEY) and partial fluorescence yield (PFY) modes, by using a photon beam incidence angle of 45°. The leakage current was measured with a Keithley picoammeter; fluorescence photons were detected using a Bruker XFlash® 4010 fluorescence detector in the S Kα or Fe Kα photon energy windows for S K-edge and Fe K-edge, correspondingly. An energy step of 0.2 eV was employed for these measurements.

3. Results and Discussion

3.1. HAXPES

3.1.1. Pyrite

Fig. 1 shows the HAXPES detail spectra of the Fe 2p, O 1s, S 2p and valence band (VB) energy regions of pyrite samples abraded in air (upper panels) or etched in 0.5 M ferric chloride solution (bottom panels), as measured using various excitation photon energies. The spectra are normalized to the maximum intensity value for comparison of peak shape. Peak broadening in spectra measured with higher excitation energies is ascribed to increased X-ray line widths monochromatized with the Si(1 1 1) crystal. This effect can be especially seen in the spectra measured with 6 keV excitation energy [39]. The Fe 2p spectra show a narrow peak at 707.2 eV which is recognized as a Fe $2p_{3/2}$ signal from low-spin Fe(II) in the pyrite lattice. A second Fe $2p_{3/2}$ contribution found at a higher binding energy (BE) is mainly due to a multiplet structure

ACCEPTED MANUSCRIPT

(four maxima plus satellite) with a highest intensity at ~709.8 eV from surface Fe(III) oxyhydroxides [17-22]. The presence of this Fe 2p feature is in agreement with the O 1s spectra containing an O^{2-} contribution (530.4 eV), which reduces in spectra taken with increasing excitation energy and, therefore, probing depth. Minor contributions from Fe(III)-S and high-spin Fe(II)-S species [22] may be roughly fitted by one maximum at about 708.8 eV. Additional oxygen species that can be identified in the O 1s spectra derive from water adsorbed to pyrite (533.5 eV), ferric hydroxides (535.5 eV, not in electronic equilibrium with pyrite), and oxygen in carbonaceous contamination and OH groups (~532 eV).

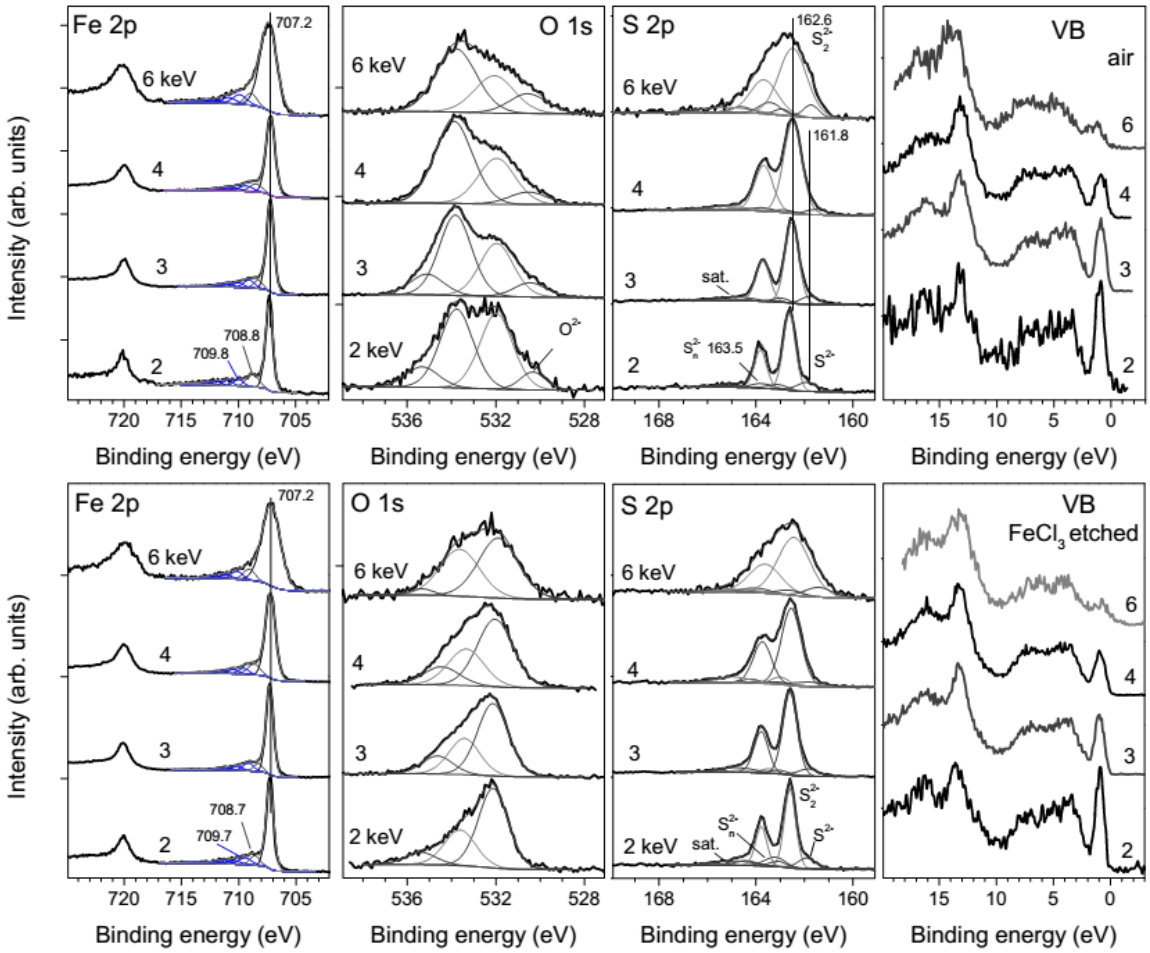

Fig. 1. Hard X-ray photoemission spectra of pyrite samples abraded in air (upper panels) and etched in 0.5 M $FeCl_3$ + 0.5 M HCl solution (50 °C, 30 min). The spectra are height-normalized for comparison; figures near the spectra indicate the employed excitation energies (in keV).

The S 2p spectra are dominated by the doublet with the S $2p_{3/2}$ peak at 162.6 eV, which is due to S_2^{2-} anions in pyrite. Additional minor lines are ascribed to monosulfide (161.8 eV), and

ACCEPTED MANUSCRIPT

polysulfide (163.5 eV) and satellite at about 164.5 eV [17-24] and slightly vary with the excitation photon energy. The VB spectra are dominated by non-bonding Fe $3d^6$ orbital states in the vicinity of 2 eV below the Fermi level [5-7]. The relative intensity of this peak decreases with increasing the excitation energy owing to lower Fe 3d photoionization cross-section values [57]. The spectra from the chemically etched pyrite (lower panels) are quite similar to the abraded samples. The main differences are found in the O 1s spectra, where the contributions of O^{2-} species are not detected and contributions of adsorbed water are substantially reduced. These changes in oxygen content suggest a removal of surface Fe(III) oxide species and the formation of a more hydrophobic surface. The intensity of polysulfide species signal in the S 2p spectra slightly increases, while that of monosulfide decreases.

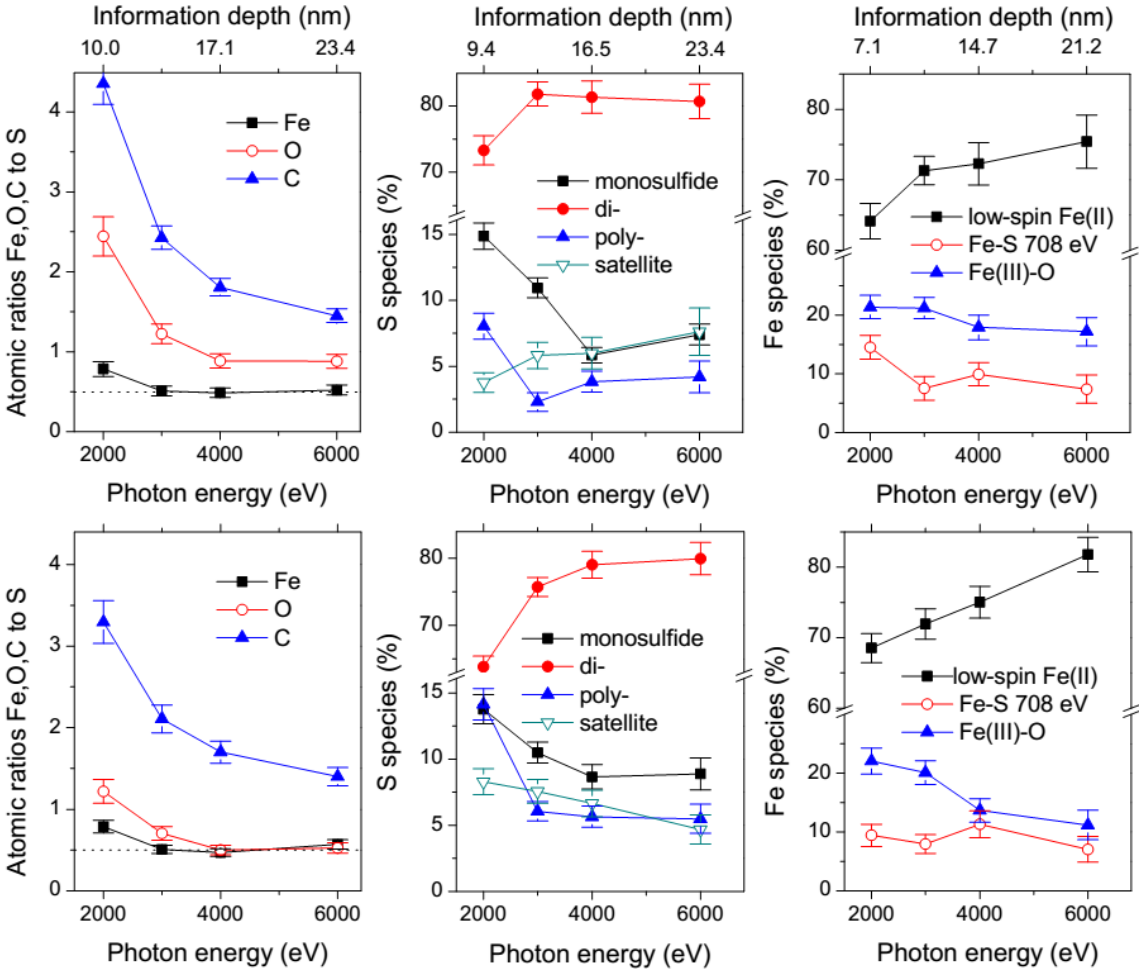

Fig. 2. Atomic ratios and the results of fitting of the S 2p and Fe 2p spectra as a function of excitation photon energy for pyrite abraded in air (upper panels) and etched in 0.5 M $FeCl_3$ + 0.5 M HCl solution.

ACCEPTED MANUSCRIPT

Intensity ratios are presented as a function of excitation energy in Fig. 2, after accounting for differences in photoionization cross section, IMFP and transmission function of the electron analyzer. The results of the S 2p and Fe 2p band fitting are also presented as a function of excitation photon energy in Fig. 2, with approximate information depths [37-42]. Whereas the calculated O/S and C/S ratios rapidly fall with increasing photon energy, the Fe/S ratios are higher at an excitation energy of 2 keV but decrease to an approximately stoichiometric value of 0.5 (at 3 keV), at which it remains at higher excitation energies. The plots demonstrate that the concentrations of oxygen, carbon and, to a lower extent, iron at the etched sample decreases relative to air oxidized pyrite. Although the deviations from FeS_2 stoichiometry are small, those are in agreement with enhanced amounts of polysulfide and reduced proportions of disulfide species. It should be mentioned that "disulfide" components with BE values ca. 162.5 eV can be attributed to terminal S atoms in S_n^{2-} ($n \geq 2$) chains, while "polysulfide" components having BE values between 163 eV and 164 eV may be inner S atoms bearing lesser negative charge in the S_n^{2-} anions [34,59]. The intensities of polysulfide and monosulfide components decrease with increasing excitation energy; some increase of the monosulfide signal at 6 keV seems to be an artifact of the line broadening.

3.1.2. Pyrrhotite

Fig. 3 (upper panels) shows the Fe 2p spectra of the in-air abraded pyrrhotite sample. The spectra can be fitted using a three-peak multiplet centered at a BE ca. 708 eV, ascribed to high-spin Fe(II) bonded to S in ferrous sulfide [21, 22]. A second Fe $2p_{3/2}$ multiplet is also present at a BE around 710 eV, which is in line with Fe(III)-O species; this second signal becomes weaker as the excitation energy increases from 2 keV to 3 keV and it slightly decreases at higher energies. The O 1s spectra reveal intense maxima at a BE of 529.9 eV, ascribed to O^{2-} in ferric oxyhydroxides. The relative intensity of this oxygen state contribution insignificantly varies with increasing photon energy, while the total concentration of oxygen diminishes, as can be seen in Fig. 4. This observation suggests that the oxidized ferric species (oxyhydroxides) occur at the surface as islands or particles with OH^- mainly at the outer shell and O^{2-} in the core. Regarding the S 2p spectra, the line of monosulfide (161.3 eV) is dominant, and the contributions of disulfide and especially polysulfide are minor and generally decrease at higher excitation energies.

ACCEPTED MANUSCRIPT

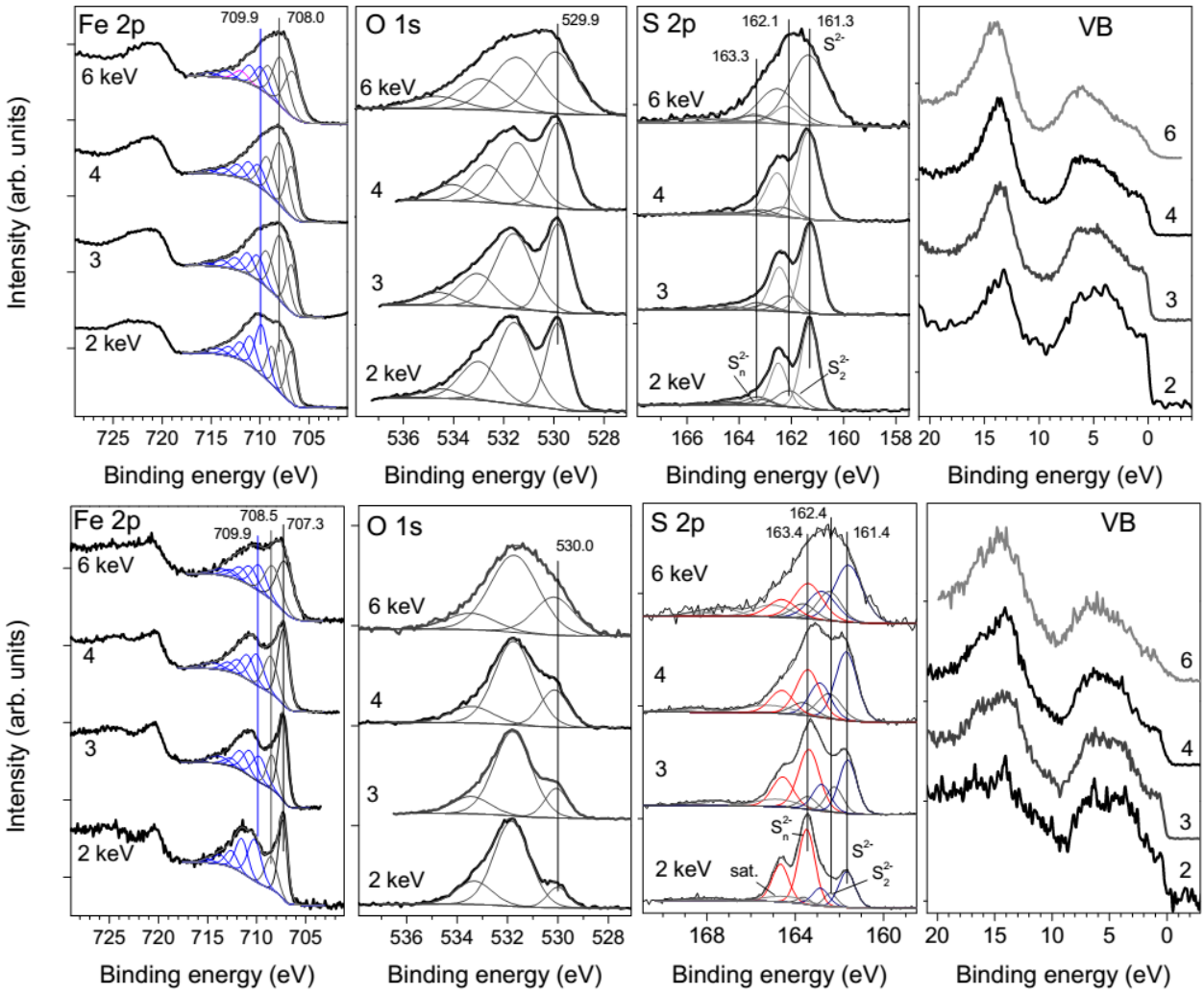

Fig. 3. HAXPES of pyrrhotite polished in air (upper) and etched in 0.5 M $FeCl_3$ + 0.5 M HCl solution (50 °C, 30 min). The spectra are height-normalized; figures near the spectra indicate the employed excitation energy (in keV).

The spectra of the sample treated in 0.5 M $FeCl_3$ + 0.5 M HCl are completely different (lower panels in Fig. 3). A narrow Fe $2p_{3/2}$ peak at 707.3 eV, which is attributable to low-spin Fe(II) in the S-rich layer [33-36], emerges along with a smaller feature conventionally approximated by one maximum located at ~708.5 eV from high-spin Fe(II)-S and possible Fe(III)-S species. Small changes of these contributions with varying photon excitation energies (when taking into account spectral resolution issues discussed above and some growth of a high-spin Fe(II)-S component) suggest that the state of iron remains nearly constant for profile depths down to ~30 nm. The S 2p spectra show that a doublet, which is ascribed to polysulfide (163.5 eV), is very strong in the 2 keV excited spectrum and that decreases with higher excitation energies (Fig. 4, lower panel). In contrast, the mono- and disulfide contributions increase in

ACCEPTED MANUSCRIPT

measurements with greater information depths but are still significantly lower when compared to the results of the air-oxidized pyrrhotite. There are also very minor signals from S-O species at the BEs above 166 eV. The atomic Fe/S ratio for this sample is high (about 1.3) at 2 keV, owing to the surface ferric oxyhydroxides, and approaches the stoichiometric ratio (~0.85) at 3 keV and higher photon energies. For the etched mineral, the Fe/S ratios are as low as 0.38 at 2 keV and 0.3 at 3 keV, and exceed 0.5 at higher energies, remaining well below the stoichiometric value. The O/S ratios slowly decrease with higher excitation energies but remain significantly high for all employed excitation energies. The O 1s spectra retain some O^{2-} signals even in the 6 keV-excited spectra, which most likely indicates that oxygen penetrates deep into the metal-deficient structure during the chemical treatment or following exposure to the atmosphere. Similar findings have been reported in Auger profiling (and other techniques) studies of acid-reacted pyrrhotites [30-32]. In the valence band spectra, peaks located at BEs in the range of 12-16 eV are derived from S 3s type states, resembling molecular orbitals of S_2^{2-} groups of pyrite, and indicate S-S bonding. The Fe 3d state peaks near the VB maximum appear weak and are probably widened and shifted as compared to pyrite.

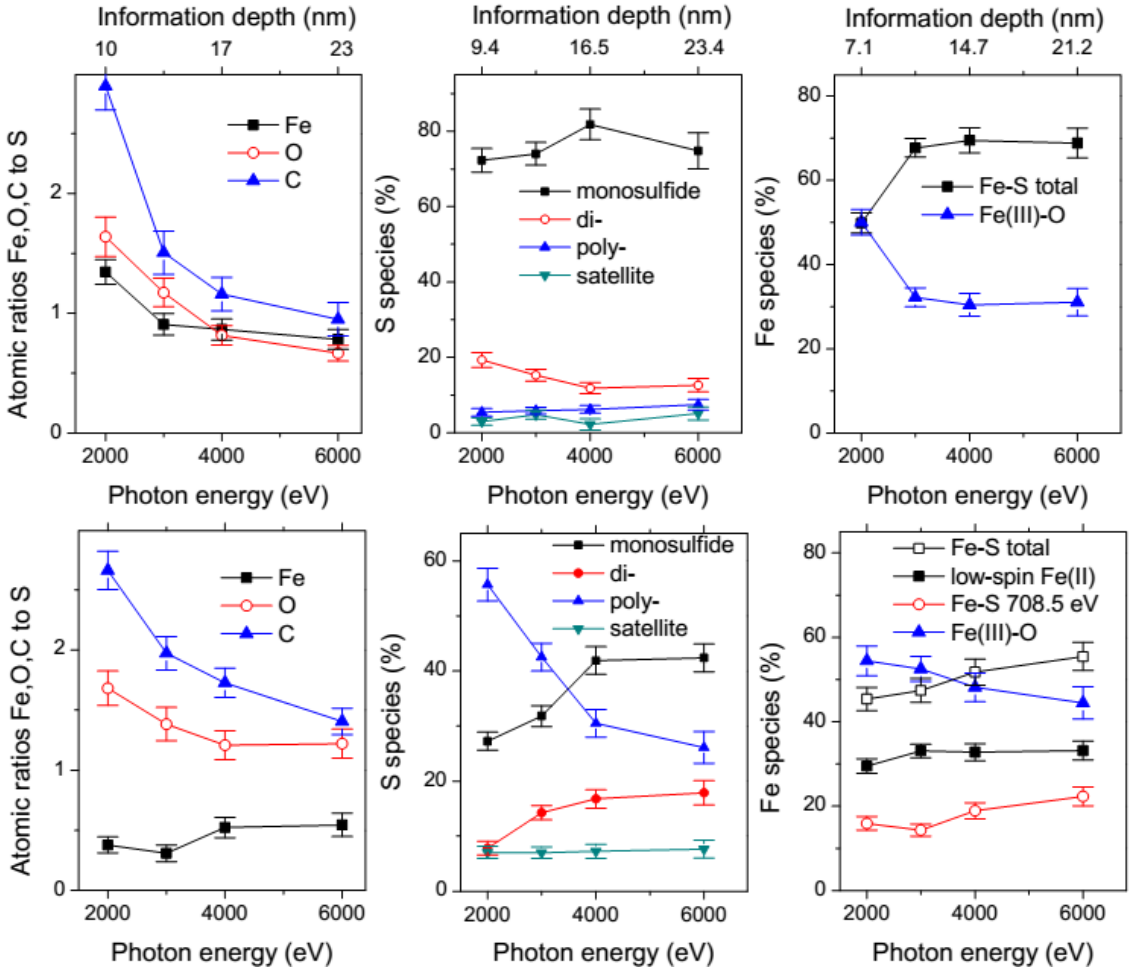

ACCEPTED MANUSCRIPT

Fig. 4. Atomic ratios and the results of fitting of the S 2p and Fe 2p spectra as a function of excitation photon energy for pyrrhotite abraded in air (upper panels) and etched in 0.5 M $FeCl_3$ + 0.5 M HCl solution (lower panels).

3.2. XANES

Fig. 5 shows S K- and Fe K-edge XANES measured simultaneously in TEY and PFY modes from pyrites oxidized in air and etched in the $FeCl_3$ solution. The leading peak *a* in the S K-XANES results from transitions from the S 1s to the antibonding S 3p states in S_2^{2-} anions; a shoulder *b* together with a small pre-edge peak *b* in the Fe K-edge spectra are commonly attributed to electron transitions from the core Fe 1s to vacant Fe 3d e_g states mixed with Fe 4p and with S 3p σ^* states (1s - 3d transitions are forbidden by dipole selection rules) [43-48]. The resonances *c* correspond to Fe 4p,s states mixed with S 3p σ^* orbitals; the peak *d* is due to transition to Fe 4p,s states [43-48], and the feature *e* can be assigned to transitions to atomic S 3p orbitals and multiple scattering resonances [45] or Fe 4sp – S 3d states [60]. The Fe K-edge XANES measured in the PFY mode do not change as a result of oxidation and etching and correspond to the bulk pyrite. In TEY mode spectra, the resonances *b* are lower for air-oxidized sample and almost disappear after the oxidative leaching; the relative intensities of the shoulder *c* are also smaller than for the bulk. The TEY mode S K-edge spectra revealed clearly different pre-edge peaks which are several times more intense relative to the absorption jump and narrower than in the PFY mode.

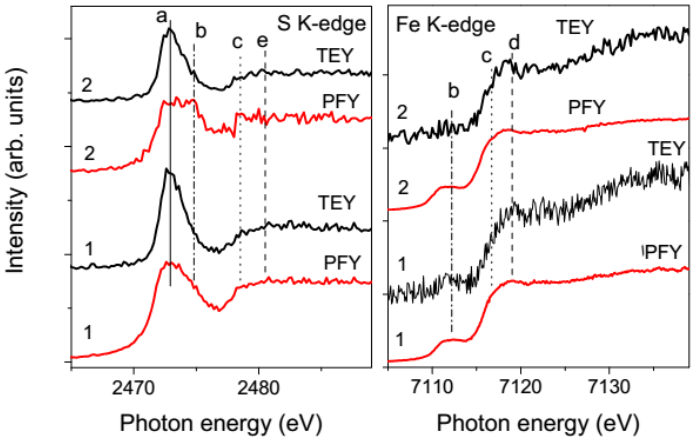

Fig. 5. S K-edge and Fe K-edge XANES from pyrite (1) abraded in air and (2) etched in 0.5 M $FeCl_3$ + 0.5 M HCl solution (30 min, 50 °C) collected in TEY and PFY modes.

The XAS spectra of NiAs-structured pyrrhotite and stoichiometric troilite FeS have been measured, calculated and analyzed in a number of studies; the spectroscopic features are largely

ACCEPTED MANUSCRIPT

similar to those in pyrite, despite different electronic structures, and their detailed description can be found in the literature [43-56]. The main differences observed in the S K-edge XANES (Fig. 6) are narrower pre-edge peaks with lower heights relative to the absorption edge, which are attributable to the absence of S-S bonding [47]. Similar to pyrite, both the S K-edge and Fe K-edge spectra collected in PFY mode did not change significantly after sample oxidation, indicating that the modified region is shorter than the probing depth of the technique. The pre-edge maxima of the Fe K-XANES of pyrrhotite almost disappeared in the spectra measured in TEY mode. Additional intensity shifted by 2-2.5 eV to higher energy relative to the main pre-edge peak arose in the S K-XANES TEY spectra that can be assigned to S-S bonding in the metal-deficient structure, as its position is close to that in pyrite.

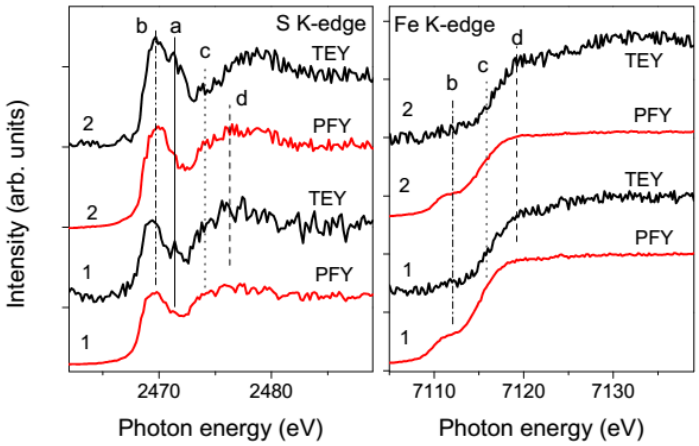

Fig. 6. S K-edge and Fe K-edge XANES from pyrrhotite (1) abraded in air and (2) etched in 0.5 M $FeCl_3$ + 0.5 M HCl solution (30 min, 50 ^{o}C) collected in TEY and PFY modes.

4. Discussion

Omitting water-derived adsorbates and carbon contamination, the HAXPES data suggests the presence of surface ferric oxyhydroxides at pyrite and pyrrhotite, probably as islands of several nm in height (Fig. 7). Additionally, the near-surface region of pyrite exhibits enhanced contents of S, polysulfide-type species and some monosulfide ions as compared to the FeS_2 composition. The thickness of this region is significantly lower than the measurement information depths of 10-15 nm [37,38], estimated at 1-2 nm for air-exposed pyrite and no greater than 3-4 nm for the ferric chloride etched mineral. Furthermore, there likely exists an extended region with insignificant compositional changes ("Fe-depleted layer") beneath the "polysulfide" layer, at least, in the etched sample. It should be noted that attempts to more precise calculate the

ACCEPTED MANUSCRIPT

thicknesses involved were limited due to multi-layered and laterally inhomogeneous compositions and complex relief of the studied mineral surfaces.

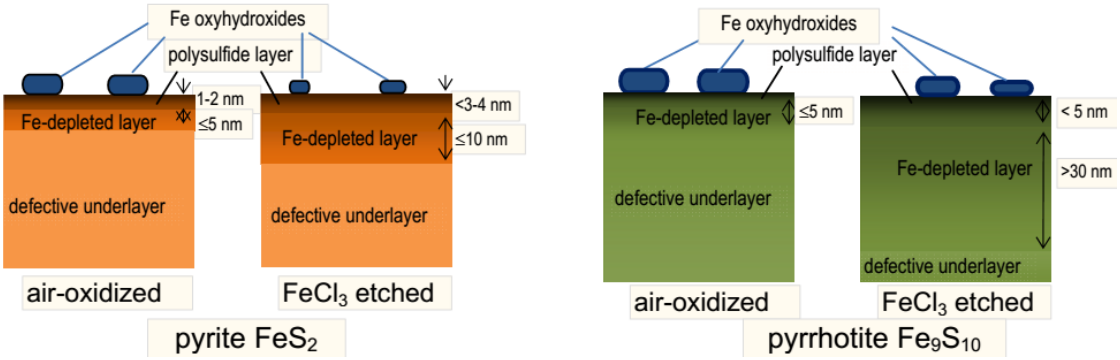

Fig. 7. Scheme illustrating layered structures of pyrite and pyrrhotite oxidized in air and etched in aqueous 0. 5 M $FeCl_3$ + HCl solution derived from HAXPES and XANES spectra

The HAXPES analysis of air-oxidized pyrrhotite revealed, underneath ferric oxyhydroxide species, the iron-deficient layer (Fig. 7), probably 1-5 nm thick, containing 20-25% of sulfur as disulfide and minor polysulfide species. After the oxidative etching, the amount of oxyhydroxides decreases, and a metal-deficient region composed of an essentially S-rich layer with polysulfide species forms, the thickness of which may be roughly estimated as less than 5 nm. Finally, the underlying layer of at least 30 nm in depth has an atomic S/Fe ratio of approximately 2 and also contains mono- and disulfide anions, Fe(II) in low-spin and high-spin state and, possibly, Fe(III), and some oxygen.

The information depths of the XANES spectra in TEY mode controlled by the penetration ranges of Auger electrons with the largest kinetic energies emitted from the absorbing atoms [61,62] are somewhat larger but still comparable to those of HAXPES at the higher excitation photon energies, while the spectra in PFY mode characterize, in fact, the bulk of the materials. The XANES data (Fig. 5, 6) show that the oxidative etching and even air oxidation moderately modify the near-surface composition of iron sulfides, in particular refractory pyrite, altering the electronic structure of the materials at depths of many tens of nanometers (Fig. 7).

The structures observed are definitely due to preferential release of iron and the formation of heavily defective metal-deficient layers comprising cation vacancies and complexes of defects, S-S bonding and possibly oxygen incorporation. This should modify the electronic properties of semiconducting metal chalcogenides, including the Fermi level pinning, carrier mobility and conductivity. Up to now, researchers have largely focused their attention on outer surface layers, while the underlying extended defective region could seriously affect surface

ACCEPTED MANUSCRIPT

processes in which the charge transport is important. We hypothesize, in particular, that such structures should take part in the inhibited anodic oxidation and oxidative leaching of pyrite, pyrrhotite and other metal sulfides [1-4, 63-66]. Noteworthy, the above phenomena arise as a result of the sample handling in atmosphere, that is, in the early stages of metal sulfide oxidation. Further work should be focused on studying detailed characteristics of the reacted layers in order to understand their role.

5. Conclusions

HAXPES and XANES characterization of pyrite and pyrrhotite revealed that the composition and chemical state of iron and sulfur varied with depth from the surface to at least several tens of nanometers as a result of oxidation of the minerals in air and the oxidative etching in Fe(III) solution. Iron is released from the metal sulfide lattice, creating strongly modified regions at pyrrhotite, whereas the compositional changes at pyrite are less pronounced. In addition to surface ferric oxyhydroxides formed at the surfaces exposed to air, several sublayers may be distinguished in the under-surface regions of the reacted iron sulfide phases. Polysulfide species are accumulated only in thin, no more than 1-4 nm in depth, outer layers. The region with smaller deviations from the stoichiometry and low, if any, concentration of polysulfide lays underneath; its dimensions widely vary for pyrite and pyrrhotite depending on the chemical treatment. In pyrrhotite samples etched in ferric chloride solution, this layer with about 30 nm or more thickness comprises mono- and disulfide anions, and low-spin Fe(II). The next, almost stoichiometric layers exhibit altered the XANES spectra in TEY mode, implying spatially extended distortion of the crystalline structures, even for chemically resistive pyrite, already after oxidation in air. We suggest that these highly defective regions are the most important in terms of the pinning of the Fermi level and near-surface charge transfer, in particular, in mineral passivation, and require further investigation.

Acknowledgements

This research was supported by the Russian Science Foundation, grant 14-17-00280, and bilateral program “German-Russian laboratory at BESSY II”. We thank HZB for the allocation of synchrotron radiation beamtime for HAXPES/XANES measurements.

ACCEPTED MANUSCRIPT

References

[1] D. Rickard, G.W. Luther III, Chemistry of iron sulfides, Chem. Rev. 107 (2007) 514−562.

[2] J.D. Rimstidt, D.J. Vaughan, Pyrite oxidation: a state of-the-art-assessment of the reaction mechanism. Geochim. Cosmochim. Acta 67 (2003) 873–880.

[3] R. Murphy, D.R. Strongin, Surface reactivity of pyrite and related sulfides, Surf. Sci. Rep. 64 (2009) 1−45.

[4] A.P. Chandra, A.R. Gerson, The mechanisms of pyrite oxidation and leaching: A fundamental perspective, Surf. Sci. Rep. 65 (2010) 293–315.

[5] K. Andersson, M. Nyberg, H. Ogasawara, D. Nordlund, T. Kendelewicz, C.S. Doyle, G.E. Brown Jr., L.G.M. Pettersson, A. Nilsson, Experimental and theoretical characterization of the structure of defects at the pyrite FeS_2 (100) surface, Phys. Rev. B 70 (2004) 70, 195404.

[6] F.W. Herbert, A. Krishnamoorthy, K.J. Van Vliet, B. Yildiz, Quantification of electronic band gap and surface states on FeS_2(100), Surf. Sci. 618 (2013) 53-61. dx.doi.org/10.1016/j.susc.2013.08.014.

[7] P. Xiao, X.L. Fan, L.-M. Liu, W.-M. Lau, Band gap engineering of FeS_2 under biaxial strain: a first principles study, Phys. Chem. Chem. Phys. 16 (2014) 24466—24472.

[8] A. Ennaoui, S. Fiechter, Ch. Pettenkofer, N. Alonso-Vante, K. Bülker, M. Bronold, Ch. Höpfner, H. Tributsch, Iron disulfide for solar energy conversion, Sol. Energy Mater. Sol. Cells 29 (1993) 289-370.

[9] C. Steinhagen, T.B. Harvey, C.J. Stolle, J. Harris, B.A. Korgel, Pyrite Nanocrystal Solar Cells: Promising, or Fool's Gold? J. Phys. Chem. Lett. 3 (2012) 2352−2356.

[10] D. Golodnitsky, E. Peled, Pyrite as cathode insertion material in rechargeable lithium/composite polymer electrolyte batteries, Electrochim. Acta 45 (1999) 335-350.

[11] S.S. Zhang, The redox mechanism of FeS_2 in non-aqueous electrolytes for lithium and sodium batteries, J. Mater. Chem. A 3 (2015) 7689–7694.

[12] C. Uhlig, E. Guenes, A.S. Schulze, M.T. Elm, P.J. Klar, S. Schlecht, Nanoscale FeS_2 (pyrite) as a sustainable thermoelectric material, J. Electron. Mater. 43 (2014) 2362-2370.

[13] E.F. Bertaut, Contribution à l'étude des structures lacunaires, Acta Crystallogr. 6 (1953) 537-561.

[14] S. Sakkopoulos, E. Vitoratos, T. Argyreas, Energy-band diagram for pyrrhotite, J. Phys. Chem. Solids 45 (1984) 923-928.

[15] A.N. Buckley, R. Woods, X-ray photoelectron spectroscopy of oxidized pyrrhotite surfaces. I. Exposure to air, Appl. Surf. Sci. 22/23(1985) 280-287.

ACCEPTED MANUSCRIPT

[16] A.N. Buckley, R. Woods, X-ray photoelectron spectroscopy of oxidized pyrrhotite surfaces. II: Exposure to aqueous solutions, Appl. Surf. Sci. 20 (1985) 472-480.

[17] J.R. Mycroft, G.M. Bancroft, N.S. McIntyre, J.W. Lorimer, I.R. Hill, Detection of sulfur and polysulfides on electrochemically oxidized pyrite surfaces by X-ray photoelectron-spectroscopy and Raman-spectroscopy, J. Electroanal. Chem. 292 (1990) 139−152.

[18] H.W. Nesbitt, I.J. Muir, X-ray photoelectron spectroscopic study of a pristine pyrite surface reacted with water-vapor and air, Geochim. Cosmochim. Acta 58 (1994) 4667−4679.

[19] C.M. Eggleston, J.J. Ehrhardt, W. Stumm, Surface structural controls on pyrite oxidation kinetics: An XPS-UPS, STM, and modeling study, Am. Mineral. 81 (1996) 1036−1056.

[20] A.G. Schaufuss, H.W. Nesbitt, I. Kartio, K. Laajalehto, G.M. Bancroft, R. Szargan, Reactivity of surface chemical states on fractured pyrite, Surf. Sci. 411 (1998) 321−328.

[21] H.W. Nesbitt, G.M. Bancroft, A.R. Pratt, M.J. Scaini, Sulfur and iron surface states on fractured pyrite surfaces, Am. Mineral. 83 (1998) 1067−1076.

[22] H.W. Nesbitt, M. Scaini, H. Hochst, G.M. Bancroft, A.G. Schaufuss, R. Szargan, Synchrotron XPS evidence for Fe^{2+}-S and Fe^{3+}-S surface species on pyrite fracture-surfaces, and their 3d electronic states, Am. Mineral. 85 (2000) 850-857.

[23] J.A. Leiro, S.S. Mattila, K. Laajalehto, XPS study of the sulphur 2p spectra of pyrite, Surf. Sci. 547 (2003) 157−161.

[24] G.U. von Oertzen, W.M. Skinner, H.W. Nesbitt, Ab initio and x-ray photoemission spectroscopy study of the bulk and surface electronic structure of pyrite (100) with implications for reactivity, Phys. Rev. B 72 (2005) 235427.

[25] A.P. Chandra, A.R. Gerson, Pyrite (FeS_2) oxidation: A sub-micron synchrotron investigation of the initial steps, Geochim. Cosmochim. Acta 75 (2011) 6239–6254.

[26] F.W. Herbert, A. Krishnamoorthy, W. Ma, K.J. Van Vliet, B. Yildiz, Dynamics of point defect formation, clustering and pit initiation on the pyrite surface, Electrochim. Acta 127 (2014) 416–426.

[27] C.F. Jones, S. LeCount, R.St.C. Smart, T.J. White, Compositional and structural alteration of pyrrhotite surfaces in solution: XPS and XRD studies, Appl. Surf. Sci. 55 (1992) 65-85.

[28] J.E. Thomas, C.F. Jones, W.M. Skinner, R.St.C. Smart, The role of surface sulfur species in the inhibition of pyrrhotite dissolution in acid conditions, Geochim. Cosmochim. Acta 62 (1998) 1555–1565.

[29] A.R. Pratt, I.J. Muir, H.W. Nesbitt, X-ray photoelectron and Auger electron studies of pyrrhotite and mechanism of air oxidation, Geochim. Cosmochim. Acta 58 (1994) 827-841.

ACCEPTED MANUSCRIPT

[30] A.R. Pratt, H.W. Nesbitt, I.J. Muir, Generation of acids from mine waste: Oxidative leaching of pyrrhotite in dilute H_2SO_4 solutions (pH 3), Geochim Cosmochim Acta 58 (1994) 5147-5159.

[31] A.R. Pratt, H.W. Nesbitt, Pyrrhotite leaching in acid mixtures of HCl and H_2SO_4, Amer. J. Sci. 297 (1997) 807-820.

[32] J.R. Mycroft, H.W. Nesbitt, A.R. Pratt, X-ray photoelectron and Auger electron spectroscopy of air-oxidized pyrrhotite: Distribution of oxidized species with depth, Geochim. Cosmochim. Acta 59 (1995) 721-733.

[33] Yu.L. Mikhlin, Ye.V. Tomashevich, G.L. Pashkov, A.V. Okotrub, I.P. Asanov, L.N. Mazalov, Electronic structure of the non-equilibrium iron-deficient layer of hexagonal pyrrhotite, Appl. Surf. Sci. 125 (1998) 73-84.

[34] Yu. Mikhlin, V. Varnek, I. Asanov, Ye. Tomashevich, A. Okotrub, A. Livshits, G. Selyutin, G. Pashkov, Reactivity of pyrrhotite (Fe_9S_{10}) surfaces: Spectroscopic studies, Phys. Chem. Chem. Phys. 2 (2000) 4393-4398.

[35] Yu.L. Mikhlin, A.V. Kuklinskiy, N.I. Pavlenko, V.A. Varnek, I.P. Asanov, A.V. Okotrub, G.E. Selyutin, L.A. Solovyev, Spectroscopic and XRD studies of the air degradation of acid-reacted pyrrhotites, Geochim Cosmochim Acta 66 (2002) 4077-4087.

[36] Yu. Mikhlin, Ye. Tomashevich, Pristine and reacted surfaces of pyrrhotite and arsenopyrite as studied by X-ray absorption near-edge structure spectroscopy, Phys. Chem. Minerals 32 (2005) 19-27.

[37] C.J. Powell, A. Jablonski, Surface sensitivity of X-ray photoelectron spectroscopy, Nucl. Instrum. Methods A 601 (2009) 54-65.

[38] S. Tanuma, H. Yoshikawa, H. Shinotsuka, R. Ueda, Calculations of mean escape depths of photoelectrons in elemental solids excited by linearly polarized X-rays for high-energy photoelectron spectroscopy, J. Electron Spectrosc. Relat. Phenom. 190, Part B (2013), 127-136. dx.doi.org/10.1016/j.elspec.2013.08.011

[39] M. Gorgoi, S. Svensson, F. Schäfers, G. Öhrwall, M. Mertin, P. Bressler, O. Karis, H. Siegbahn, A. Sandell, H. Rensmo, W. Doherty, C. Jung, W. Braun, W. Eberhardt, The high kinetic energy photoelectron spectroscopy facility at BESSY progress and first results, Nucl. Instrum. Methods A 601 (2009) 48-53. dx.doi.org/10.1016/j.nima.2008.12.244.

[40] M. Gorgoi, N. Mårtensson, S. Svensson, HAXPES studies of solid materials for applications in energy and information technology using the HIKE facility at HZB-BESSY II, J. Electron Spectrosc. Relat. Phenom. 200 (2015) 40–48.

ACCEPTED MANUSCRIPT

[41] H. Mönig, Ch.-H. Fischer, R. Caballero, C.A. Kaufmann, N. Allsop, M. Gorgoi, R. Klenk, H.-W. Schock, S. Lehmann, M.C. Lux-Steiner, I. Lauermann, Surface Cu depletion of Cu(In,Ga)Se_2 films: An investigation by hard X-ray photoelectron spectroscopy, Acta Mater. 57 (2009) 3645-3651. dx.doi.org/10.1016/j.actamat.2009.04.029.

[42] B. Ümsür, W. Calvet, B. Höpfner, A. Steigert, I. Lauermann, M. Gorgoi, K. Prietzel, H.A. Navirian, C.A. Kaufmann, T. Unold, M.Ch. Lux-Steiner, Investigation of Cu-poor and Cu-rich Cu(In,Ga)Se_2/CdS interfaces using hard X-ray photoelectron spectroscopy, Thin Solid Films, 582 (2015) 366-370.

[43] C. Sugiura, Sulfur K x-ray absorption spectra of FeS, FeS_2, and Fe_2S_3, J. Chem. Phys. 74 (1981) 215-217.

[44] C. Sugiura, Iron K x-ray absorption-edge structure of FeS and FeS_2, J. Chem. Phys. 80 (1984) 1047-1049.

[45] J.F.W. Mosselmans, R.A.D. Pattrick, G. van der Laan, J.M. Charnock, D.J. Vaughan, C.M.B. Henderson, C.D. Garner, X-ray absorption near-edge spectra of transition metal disulfides (pyrite and marcasite), CoS_2, NiS_2 and CuS_2, and their isomorphs FeAsS and CoAsS, Phys. Chem. Minerals 22 (1995) 311-317.

[46] D. Li, G.M. Bancroft, M. Kasrai, M.E. Fleet, X. Feng, K. Tan, S K- and L-edge X-ray absorption spectroscopy of metal sulfides and sulfates: applications in mineralogy and geochemistry, Can. Mineral. 33 (1995) 949-960.

[47] M. Womes, R.C. Karnatak, J.M. Esteva, I. Lefebvre, G. Allan, J. Olivier-Fourcade, J.C. Jumas, Electronic structures of FeS and FeS_2: X-ray absorption spectroscopy and band structure calculations, J. Phys. Chem. Solids 58 (1997) 345-352.

[48] K.E.R. England, J.M. Charnock, R.A.D. Pattrick, D.J. Vaughan, Surface oxidation studies of chalcopyrite and pyrite by glancing-angle X-ray absorption spectroscopy (REFLEXAFS), Mineral. Mag. 63 (1999) 559-566.

[49] S.P. Farrell, M.E. Fleet, I.E. Stekhin, A. Kravtsova, A.V. Soldatov, X. Liu, Evolution of local electronic structure in alabandite and niningerite solid solutions [(Mn,Fe)S, (Mg,Mn)S, (Mg,Fe)S using sulfur K and L-edge XANES spectroscopy, Am. Mineral. 87 (2002) 1321-1332.

[50] P.A. O'Day, N. Rivera Jr., R. Root, S.A. Carroll, X-ray absorption spectroscopic study of Fe reference compounds for the analysis of natural sediments, Am. Mineral. 89 (2004) 572-585.

[51] L.A.J. Garvie, P.R. Buseck, Unoccupied states of pyrite probed by electron energy-loss spectroscopy (EELS), Am. Miner. 89 (2004) 485-491.

[52] A.N. Kravtsova, I.E. Stekhin, A.V. Soldatov, X. Liu, M.E. Fleet, Electronic structure of MS (M = Ca,Mg,Fe,Mn): X-ray absorption analysis, Phys. Rev. B 69 (2004) 134109.

ACCEPTED MANUSCRIPT

[53] A.V. Soldatov, A.N. Kravtsova, M.E. Fleet, S.L. Harmer, Electronic structure of MeS (Me= Ni,Co,Fe): X-ray absorption analysis, J. Phys. Cond. Matt. 16 (2004) 7545-7556.

[54] M.E. Fleet, XANES spectroscopy of sulfur in Earth materials, Can. Mineral. 43 (2005) 1811-1838.

[55] T. Oguchi, H. Momida, First-principles study of X-ray absorption spectra of FeS_2, J. Phys. Soc. Jpn. 82 (2013) 065004.

[56] A. Kitajou, J. Yamaguchi, S. Hara, S. Okada, Discharge/charge reaction mechanism of a pyrite-type FeS_2 cathode for sodium secondary batteries, J. Power Sources 247 (2014) 391-395.

[57] M.B. Trzhaskovskaya, V.I. Nefedov, V.G. Yarzhemsky, Photoelectron angular distribution parameters for elements Z= 1 to Z= 54 in the photoelectron energy range 100–5000 eV, At. Data Nucl. Data Tables 77 (2001) 97–159.

[58] M.B. Trzhaskovskaya, V.I. Nefedov, V.G. Yarzhemsky, Photoelectron angular distribution parameters for elements Z= 55 to Z= 100 in the photoelectron energy range 100–5000 eV, At. Data Nucl. Data Tables 82 (2002) 257–311

[59] A.N. Buckley, H.J. Wouterland, P.S. Cartwright, R.D. Gilbuckley, Core electron binding energies of platinium and rhodium polysulfides, Inorg. Chim. Acta 143 (1988)77-80.

[60] T. Ollonqvist, R. Perälä, J. Väyrynen, Unoccupied electronic states of the FeS_2(100) surface studies by inverse photoemission, Surf. Sci. 377-379 (1997) 201-205.

[61] A. Erbil, G.S. Cargill III, R. Frahm, R.F. Boehme, Total-electron-yield current measurements for near-surface extended x-ray-absorption fine structure, Phys. Rev. B 37 (1988) 2450-2464.

[62] S.L.M. Schroeder, Towards a ‘universal curve’ for total electron-yield XAS, Solid State Commun. 98 (1996) 405-409.

[63] Y. Mikhlin, Y. Tomashevich, A. Kuklinskiy, D. Shipin, I. Asanov, A. Okotrub, V. Varnek, N. Bausk, Passivation of sulfide minerals: are the metal-deficient layers responsible? In Electrochemistry in mineral and metal processing VI, eds F. M. Doyle, G. H. Kelsall, and R. Woods, The Electrochem. Soc. Proc. 18 (2003) 96-107.

[64] Yu.L. Mikhlin, Ye.V. Tomashevich, I.P. Asanov, A.V. Okotrub, V.A. Varnek, D.V. Vyalikh, Spectroscopic and electrochemical characterization of the surface layers of chalcopyrite ($CuFeS_2$) reacted in acidic solutions, Appl. Surf. Sci. 225 (2004) 395-409.

[65] P.R. Holmes, F.K. Crundwell, Polysulfides do not passivate: Results from pyrite and implications for other sulfide minerals, Hydrometallurgy 139 (2013) 101–110. doi:10.1016/j.hydromet.2013.07.006

[66] R.H. Lara, J. Vazquez-Arenas, G. Ramos-Sanchez, M. Galvan, L. Lartundo-Rojas, Experimental and theoretical analysis accounting for differences of pyrite and chalcopyrite

ACCEPTED MANUSCRIPT

oxidative behaviors for prospective environmental and bioleaching applications, J. Phys. Chem. C 119 (2015) 18364−18379.

ACCEPTED MANUSCRIPT

Figure captions

Fig. 1. Hard X-ray photoemission spectra of pyrite samples abraded in air (upper panels) and etched in 0.5 M $FeCl_3$ + 0.5 M HCl solution (50 $^{\circ}$C, 30 min). The spectra are height-normalized for comparison; figures near the spectra indicate the employed excitation energies (in keV).

Fig. 2. Atomic ratios and the results of fitting of the S 2p and Fe 2p spectra as a function of excitation photon energy for pyrite abraded in air (upper panels) and etched in 0.5 M $FeCl_3$ + 0.5 M HCl solution.

Fig. 3. HAXPES of pyrrhotite polished in air (upper) and etched in 0.5 M $FeCl_3$ + 0.5 M HCl solution (50 $^{\circ}$C, 30 min). The spectra are height-normalized;figures near the spectra indicate the employed excitation energy (in keV).

Fig. 4. Atomic ratios and the results of fitting of the S 2p and Fe 2p spectra as a function of excitation photon energy for pyrrhotite abraded in air (upper panels) and etched in 0.5 M $FeCl_3$ + 0.5 M HCl solution (lower panels).

Fig. 5. S K-edge and Fe K-edge XANES from pyrite (1) abraded in air and (2) etched in 0.5 M $FeCl_3$ + 0.5 M HCl solution (30 min, 50 $^{\circ}$C) collected in TEY and PFY modes.

Fig. 6. S K-edge and Fe K-edge XANES from pyrrhotite (1) abraded in air and (2) etched in 0.5 M $FeCl_3$ + 0.5 M HCl solution (30 min, 50 ^{o}C) collected in TEY and PFY modes.

Fig. 7. Scheme illustrating layered structures of pyrite and pyrrhotite oxidized in air and etched in aqueous 0. 5 M $FeCl_3$ + HCl solution derived from HAXPES and XANES spectra